

Optimized design and development of a vehicle-mounted vertical axis wind turbine for defense cut-off locations and its performance analysis

M. Priyadharsini, Sunil Kumar Gupta, Manoj Gupta

Department of Electrical and Electronics Engineering, Poornima University, Jaipur, India

Article Info

Article history:

Received Apr 28, 2024

Revised Feb 15, 2025

Accepted Mar 1, 2025

Keywords:

Axial flux permanent magnet

Cut-off locations

Magnetic levitation

Renewable energy

Swept area

Tip speed ratio

Vertical axis wind turbine

ABSTRACT

This paper presents a vehicle-mounted vertical-axis wind turbine (VAWT) designed to generate power in motion and at cut-off locations. Particularly, its application to military vehicles is explored to provide uninterrupted electrical power for radio communication equipment and lighting needs in remote areas. The design uses a helical wind turbine for its compactness, lightweight, and suitability for vehicle mounting without heavy support structures. These turbines have low starting wind speeds, minimal vibration, portability, affordability, and low maintenance requirements. Utilizing fiberglass blades, the turbine unit measures 103 mm in height and 27.5 mm in diameter, achieving optimal rpm and torque for given wind speeds. Operating within the wind speed range of 10 km/h to 40 km/h, the VAWT produces an output voltage ranging from 5 V to 55 V, with a maximum wind turbine power output of 1120 watts at a wind speed of 12 m/s. The final generator output power obtained with the above wind turbine output of 1120 watts is 352 watts. A prototype unit has been tested and mounted on an all-terrain vehicle for evaluation. The paper provides detailed design steps, calculations, and insights for optimizing performance and facilitating large-scale implementation in the future.

This is an open access article under the [CC BY-SA](#) license.



Corresponding Author:

Sunil Kumar Gupta

Department of Electrical and Electronics Engineering, Poornima University

Jaipur, India

Email: sunil.gupta@poornima.edu.in

1. INTRODUCTION

The depletion of conventional energy sources and the ever-increasing demand for energy due to industrialization have spurred significant research on renewable energy sources, harnessing primary and environmentally friendly natural sources such as solar power and wind energy. Among these, wind energy stands out as one of the fastest-growing sources for electricity generation. Wind turbines play a crucial role in this process, converting the mechanical energy inherent in wind into electrical energy.

The fundamental concept of wind energy generation involves utilizing the kinetic energy of wind to propel a wind turbine, thereby transforming the wind's kinetic energy into rotational kinetic energy. This rotational energy is then converted into electrical energy through the use of generators, with the output power supplied to electrical equipment. Axial flux generators, operating as permanent magnet alternators, are integral components in this setup. These generators feature an air gap surface perpendicular to the rotating axis, generating magnetic fluxes parallel to the axis. Axial flux permanent magnet (AFPM) machines with coreless topology offer distinct advantages over conventional permanent magnet machines, delivering high power, torque-to-weight ratios, and geometrically higher aspect ratios [1]-[11]. In scenarios such as cut-off locations,

where a constant power source is essential for operating communication equipment, reliance solely on storage batteries becomes inadequate. The demand calls for energy generation setups that are portable, lightweight, and independent of fuel requirements for long-distance and high-altitude operations. Renewable energy sources such as solar, portable hydropower, and wind power generators emerge as suitable solutions for such environments.

This paper presents a wind turbine model that is implemented on a moving vehicle and not in a fixed location, which is unique in its design. The paper uses a fiberglass material for the blade design to reduce the weight of the system. The efficiency of the wind turbine is improved by optimizing the angle of attack, swept area with an angle of (135-180) degrees, with a minimum of two blades, while other designs use 4 blades. The drag force reduction, along with soft braking, which is unique for small-scale wind turbine units, is practically implemented in the prototype model, while other work presents only simulation results [12]. The wind turbine uses no ball bearings but magnetic levitation to reduce the frictional loss, self-starting torque, and wear and tear of the wind turbine. The design presented is a functional model of a vertical-axis wind turbine specifically tailored for mounting on vehicle rooftops. The envisioned turbine is characterized by its lightweight construction, compact size, ease of installation, and low-cost scalability for large-scale production. The paper initially presents the design methodology in steps, optimization of various design parameters, analysis of performance with the prototype model, and its implementation in the field of operation.

2. DESIGN AND DEVELOPMENT

The prototype developed employs an AFPM design with an ironless rotor, offering a high power-to-torque ratio, torque-to-weight ratio, mechanical strength, and power density without increasing the generator's size. Such attributes render it suitable for deployment in various moving vehicles, including ships, for wind power generation. Operationally, wind turbines function as the wind moves, with the dynamic energy of the wind causing the turbine blades to rotate the rotor shaft, thereby generating electricity. In the case of vertical-axis wind turbines, the generator is connected to a gearbox to increase the speed.

Magnetic levitation is a method in which an object is connected without any mechanical support other than magnetic force. The magnetic force from the permanent magnet is used to balance the gravitation force and to lift the object as shown in Figure 1. This idea is applied in a wind turbine to reduce friction losses during electricity generation. In a vertical-axis wind turbine (VAWT), the blades are connected to the rotor using permanent magnets (PM), which generate a magnetic force to lift the sharp blades. This reduces the wear and tear between the blade and the ball bearing as well as minimizes the energy loss. Using the principle of magnetic levitation, the frictional loss in a vertical-axis, vehicle-mounted wind turbine is reduced. This design is capable of operating at both low and high wind speeds (2.7 m/s to 12 m/s), increases efficiency by 20% [13] compared to conventional methods, and reduces failure rates by up to 80–90% in prototype testing. Vertical-axis wind turbines (VAWTs) are classified based on their primary driving force: lift or drag [14]. Based on lift, VAWTs are with various shapes like straight, helical, and curved. compared to straight-blade VAWT, the helical blade shown in Figure 2 gives better performance with lesser noise emission [15]. The horizontal axis wind turbine (HAWT) is used in marine turbines and vehicles for low power fluctuation. The blades are made with NACA0018 airfoils for small to medium-scale vertical-axis wind turbines. In HAWT, rotors and generators are arranged vertically on a shaft for mechanical support and stability. The helical turbine design does not require a strong supporting tower; therefore, it is easy to transport and assemble in a cut-off post. The HAWT has a low starting wind speed and low vibration.

The axial-flux permanent magnet (AFPM) generator has a high torque density, high efficiency, and compact structure. This generator gives high power density with less space and weight. In a cut-off post, space and weight are critical parameters; therefore, the axial flux permanent magnet (AFPM) generator is suitable for high power-density applications. In the axial flux type generator model with a double-sided rotor, core coreless armature, and non-overlapping concentrated coils are used. In an AFPM, the rotor is made of neodymium-iron-boron permanent magnets, and the stator is a coreless armature, similar to those in other generators. It works under Faraday's law of electromagnetic induction.

In AFPM [16]-[24], the magnetic fields are parallel to the axis of rotation, and the rotor and starter are with co-axial discs and work mostly in wind turbines with moderate torque capacity. In this prototype, magnetic soft braking is implemented. In this method, two copper plates are placed to hold the magnets. The magnets are permanent magnets, and the braking reference angular velocity is 13 m/s. Figure 3 shows the double-sided rotor AFPM generator, and its flux distribution is shown in Figure 4.

The prototype incorporates the soft braking system with magnetic braking to control the angular velocity of the wind turbine, unlike conventional methods. A current sensing circuit is connected to detect the current above the reference speed limit, and it is limited to 12 m/s. The developed VAWT prototype with helical blades is cost-effective and produces 1120 watts at 12 m/s wind speed, and it is lightweight, compact, and easy to transport and mount on the vehicle rooftop. This paper presents the design and development of the

prototype model in sequential steps for building a successful scaled-up model for easy mass production of the units and also for further optimization of its performance as a future scope. The design methodology is shown in Figure 5, which is adopted for the prototype VAWT design, and the developed VAWT working is shown in Figure 6.

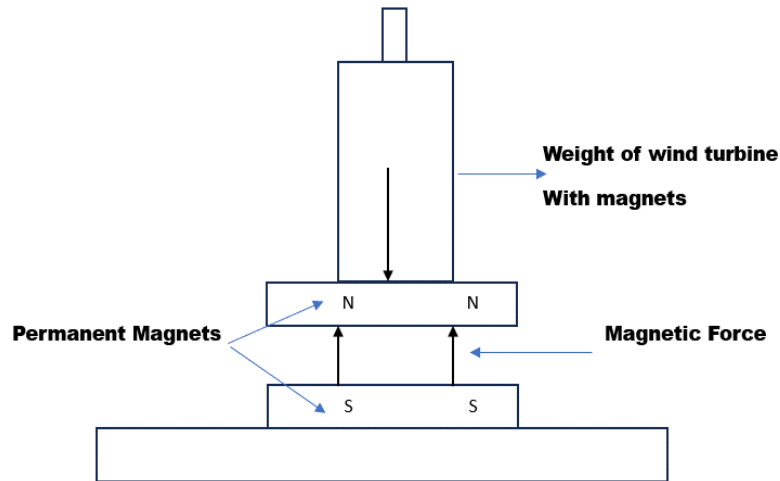


Figure 1. Magnetic levitation [13]



Figure 2. Helical wind turbine blade

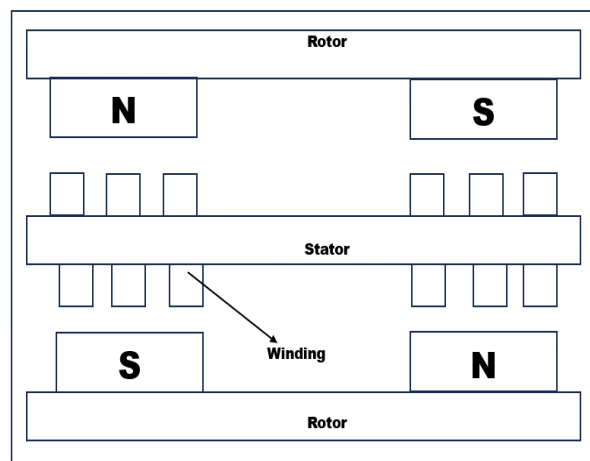


Figure 3. Double-sided rotor AFPM generator

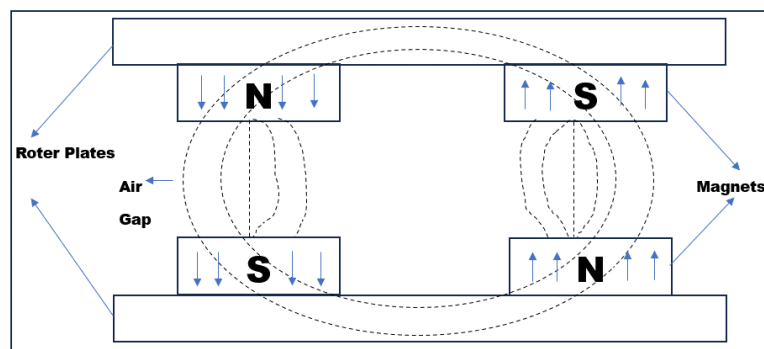


Figure 4. Flux distribution in AFPM generator

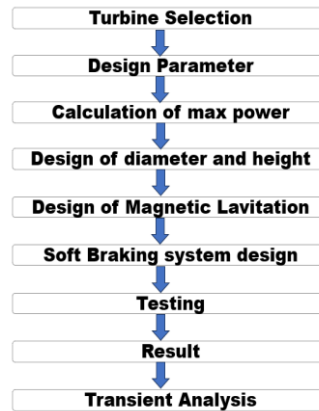


Figure 5. Design methodology of VAWT

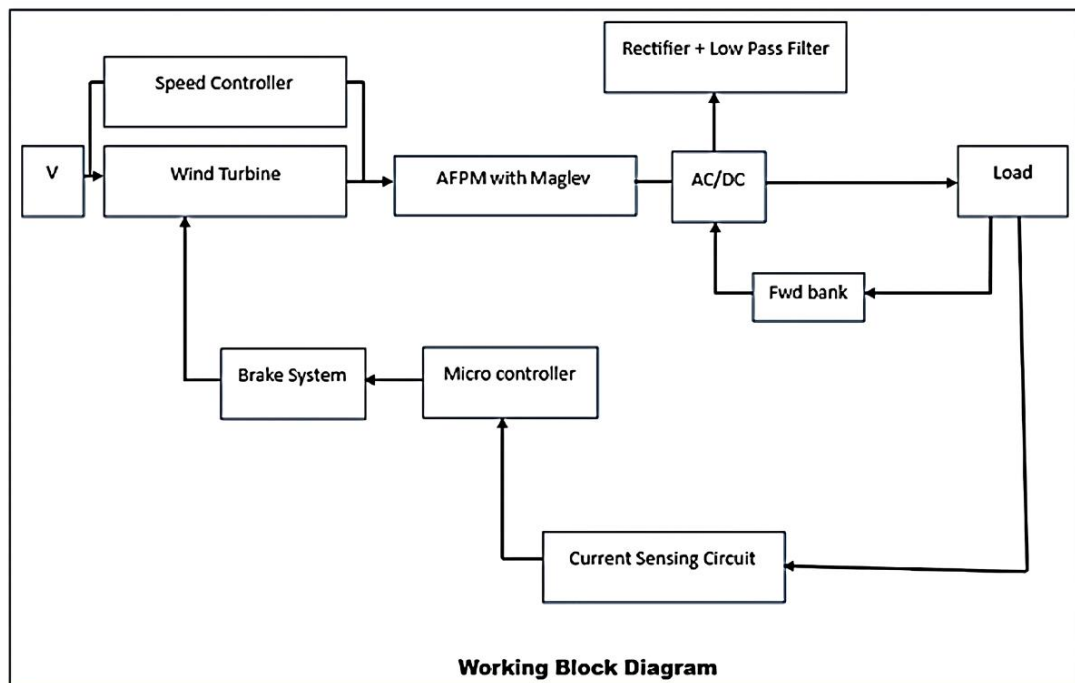


Figure 6. Prototype block diagram

2.1. Wind turbine

The design parameters for a vertical axis wind turbine are a) tip speed ratio, b) number of blades, c) blade chord, d) swept area, e) maximum power, f) power coefficient, g) solidity, and h) initial angle of attack.

a) Tip speed ratio [TSR]
The power coefficient depends on the tip speed ratio. It is defined as the ratio between the tangential speed at the blade tip and the actual wind speed [11].

$$TSR = \frac{R\omega}{V_0} \quad (1)$$

Where ω = angular velocity in rad/s, R = rotor radius in meters, and V_0 = atmospheric wind speed in m/s. The prototype model is designed to have a TSR value between 2.3 to 3.5 for an angle of 135° to 180° .

b) Number of blades [N]

The number of blades decides the smoothness of rotor operation and solidity. More blades may increase the interference between blades and affect the lift and drag forces. Therefore, it gives too optimistic results. A smaller number of blades will provide better self-starting characteristics. The prototype turbine has

two similar helical blades with 180° torsion, and both blades are placed in such a way that to have 360° of sweep area. The blades are made up of carbon fiber composite and assembled on a 1.03 m steel shaft.

c) Blade chord [c]

The chord is the blade length between the leading edge and the trailing edge of the blade. The blade curvature and thickness are defined as a percentage of the chord. The prototype is designed to have a chord length of 830 mm. Figure 7 shows the CAD diagram of the blade designed for the prototype VAWT.

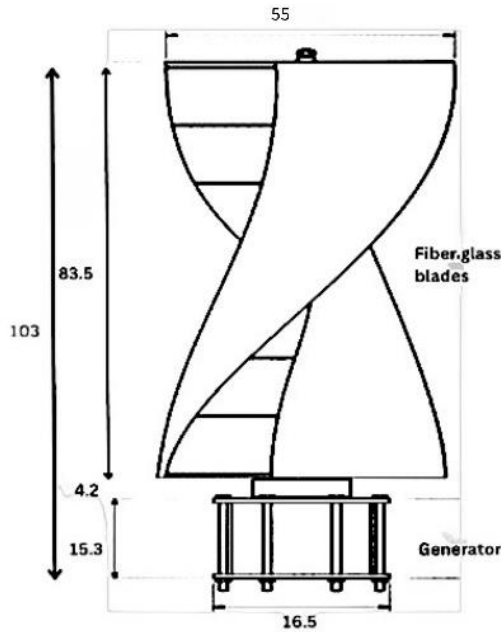


Figure 7. 2D sketching of the blade

d) Swept area [A]

The swept area is defined as the portion of air that encloses the turbine and causes the rotor to rotate on its axis. In a helical vertical axis wind turbine, the swept area has a cylindrical shape, and it can be calculated as (2), where D is the diameter of the rotor = 0.55 m and h is the height of the rotor = 1.03 m.

$$A = (D \times h) \text{ in } m^2 \quad (2)$$

e) Maximum power [Pmax]

The maximum power from the vertical axis wind turbine is (3), where ρ (air density) = 1.23 kg/m³, A = swept area in m², and V_i = inlet wind velocity in m/s.

$$P_{max} = \frac{1}{2} \rho \cdot A \cdot V_i^3 \text{ in watts} \quad (3)$$

f) Power coefficient [Cp]

It is defined as the ratio of captured mechanical power by the blades and available power in the wind. For HAWT, the limit is 16/27. The power coefficient is denoted as Cp.

g) Solidity [σ]

This solidity is defined as the ratio between the total blade area and the projected area. It is a non-dimensional parameter as shown in (4), where c is the chord length, N is the number of blades, and R is the radius of the rotor. In HAWT, the solidity $\sigma \geq 0.4$, and in the designed prototype it is 0.961.

$$\sigma = \frac{N \cdot c}{22\pi R} \quad (4)$$

h) Initial angle of attack [α]

The initial angle of attack is the angle at which the relative wind meets the blade. The positive angle of attack increases the angular speed range, but the negative angle of attack reduces the angular speed range. In the prototype unit, the angle of attack is set at 0° .

2.2. Magnetic levitation

In the prototype, the magnets are selected based on the strength of the magnetic force that is required to counteract the weight of the wind turbine rotor. The magnetic strength depends on the selection of magnetic material. The permanent magnet selected for the design is an NdFeB magnet with an outer diameter of 10 mm and an inner diameter of 5 mm. These are ring-shaped magnets with nickel plated.

$$\begin{aligned}\text{Total force } F &= 0 \\ m \cdot g - F_m &= 0 \\ F_m &= m \cdot g\end{aligned}$$

Where, F_m is a strength of magnetic force, m is total mass of the wind rotor to be levitated, and g is the gravitational force. In this prototype model weight is 3 kg and the force is 29.43 Newtons. The design uses two Neodymium magnets between the stator and rotor with a 5 mm air gap.

2.3. Generator

The prototype unit is designed with an axial flux permanent magnet synchronous generator (AFPMMSG) with a double-sided rotor. The generator is constructed using an ironless rotor with a magnetic pull between the magnets. There are 4 poles, and each rotor has two of them. The stator of AFPM is a slotless core wound with 800 turns. There are 10 units, each unit consists of 80 turns. The units are placed in such a way that the adjacent unit has opposite polarity, and the magnetic field is 5 mWb. The generator has a maximum speed of 500 rpm, producing a pulsating DC output that is subsequently converted to pure DC using a converter circuit. Figure 8 shows the coil and magnet arrangement of AFPM.

2.4. Maximum power point tracking [MPPT]

The maximum power point tracking is a technique to increase the conversion efficiency of wind turbines. The instantaneous change in the wind is important to find the optimum generator speed that produces maximum wind energy. MPPT controllers help in adjusting the voltage and current according to the wind speed to produce a maximum amount of power from the wind turbine for higher efficiency. More power generation and lower cost over time. The prototype unit uses a converter with an MPPT of 55 V and 500 W, single phase, and with reverse current protection. The voltage and power rating of the converter is selected as per the wind turbine generator output specifications.

2.5. Rectifier

The desired output voltage is obtained using the PWM model, and the output of the PWM is adjusted with the applied gate signal. The controller is designed for low-side N-channel MOSFET switching regulators. The controller turns ON with 2.97 V, and the maximum voltage is up to 40 V. The maximum switching frequency is 100 Hz, and the inductance and capacitance values were calculated for the switching frequency. Figure 9 shows the rectifier with a low-pass filter used in the prototype design.

2.6. Soft braking design

Using the magnet and current detection circuit, the braking system develops smooth and controlled braking at high speeds in a wind turbine. The circuit gives real-time monitoring with the help of a microcontroller. The current detection circuit is connected between the generators and the magnetic brake circuit. The current transformer is connected in the braking system to avoid the interference between each component [25]-[34].

The moment of inertia using braking torque in a controlled magnetic braking system is given by (5), where J = moment of inertia of the blade in kgm^2 , P_w = wind power in watts, T_r = friction torque in Nm, T_m = permanent magnetic brake torque in Nm, D_f = decision function with respect to time and speed, D_f is proportional to $(\alpha (\omega_A - \omega_r))$. Where, $\alpha = 10^\circ$ in this prototype design, ω_A = actual wind speed m/s, and ω_r = reference wind speed m/s.

$$J = P_w - T_r - T_m \cdot D_f \quad (5)$$

The decision function will activate when the actual wind speed exceeds the reference speed. The braking torque can be written as (6), where Q_m = magnetic field by the permanent magnet, Q_s = magnetic field by the copper plate, and d = distance between the copper plate and magnet.

$$T_m = \frac{(Q_m \cdot Q_s)}{(4\pi\mu d^2)} \quad (6)$$

The prototype block diagram shown in Figure 10 shows the microcontroller with a current sensing circuit connected to sense at 13 m/s and activate the system. The copper plate and magnet are connected to a servo motor. The servo motor gives input from the current sensing circuit and activates the braking system at 13 m/s as shown in Figure 11. This system is applicable up to 1.2 kW power in a small-scale vertical-axis wind turbine with DC output. In this prototype, the permanent magnet is designed to have a magnetic field strength of 6 mWb [35], [36]. The magnetic field in the copper plate depends on the current limit, and the plate gets magnetized above 20 A. The brake system gets activated.

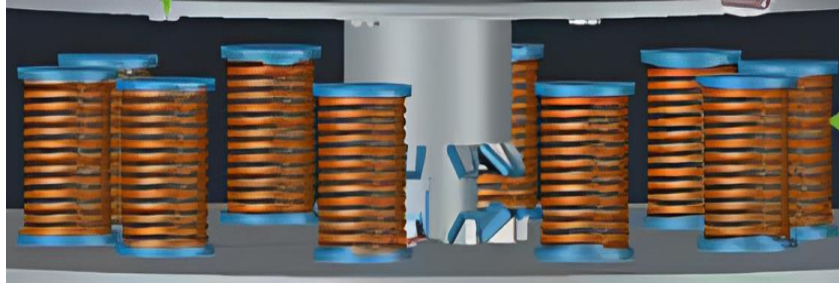


Figure 8. Shows coil and magnet arrangement of AFPM [17]

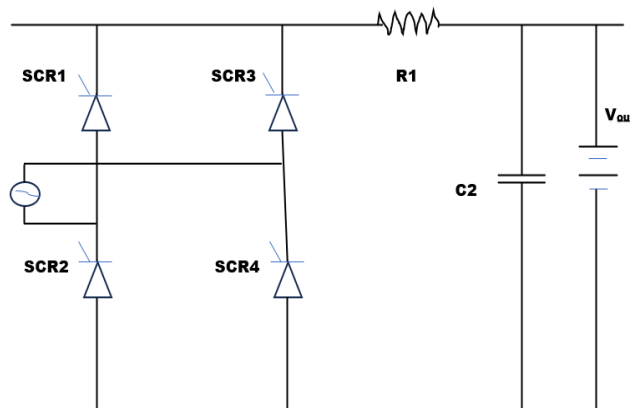


Figure 9. Shows the rectifier with low-pass filter

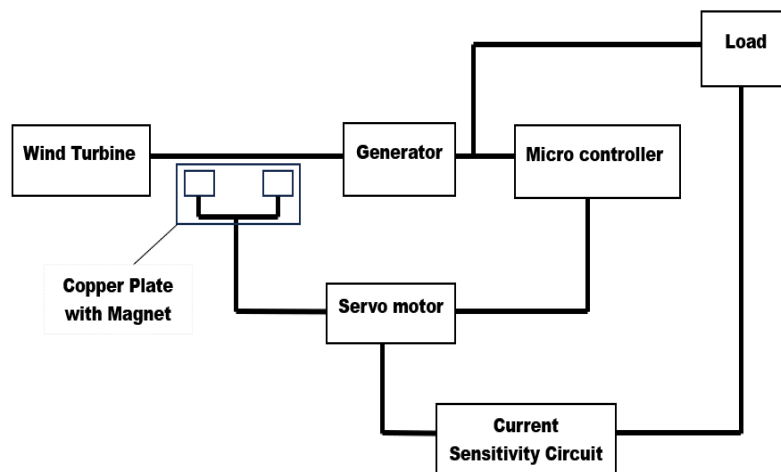


Figure 10. Block diagram of the prototype

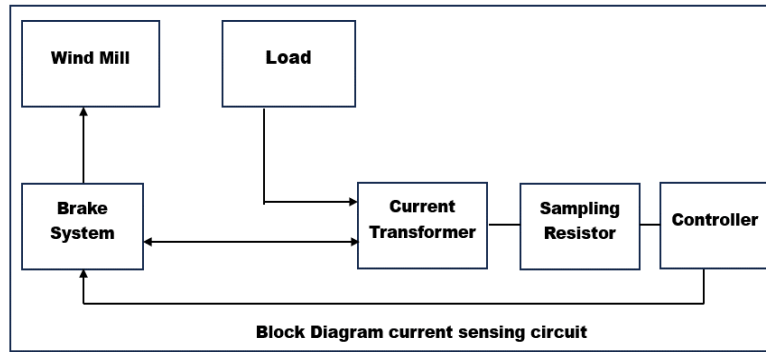


Figure 11. Current sensing circuit for soft braking

2.7. Prototype model

The initial prototype unit was integrated in the laboratory, which includes wind blades, a generator, a DC to DC converter, and LCD display units for measuring the converter voltage and current. The testing was carried out with a high-speed blower to simulate wind inside the laboratory and rotate the blades for measuring the wind turbine's voltage output. Figure 12 shows the wind turbine integrated at the laboratory for testing and measurement. Figure 13 shows the constructed prototype model and its integration to the vehicle for field trial, along with MPPT and the vehicle battery connected.



Figure 12. Wind turbine integrated



Figure 13. Vehicle-mounted VAWT

3. CALCULATION AND RESULTS

3.1. Lift and drag force

There are two methods of extracting power from wind, and they depend on the aerodynamic force used. The drag type extracts less power from the wind but with high torque. Mostly used in VAWT with a helical blade due to its low starting speed. The other type is lift type, which requires an additional system for the initial rotation, mostly used in VAWT with a Darrieus turbine. In this prototype, the main aim is to reduce the starting speed, and the helical wind turbine is selected. The experimental improvement shows that with the angle of attack of $10^\circ - 15^\circ$, the drag force is negligible. Both forces can be written as (7),

$$\text{Lift force } d_L = \frac{1}{2} \times C_L \times \rho \times W^2 \times C \times d_r \quad (7)$$

3.2. Power

The kinetic energy of the wind as shown in (8), where m = mass flow rate of blades in helical wind turbine, $m = \rho A V_w$, where, A = area of cylindrical helical wind turbine, $A = 2\pi R h$, where R = radius of rotor, H = height of rotor, V_w = wind velocity.

$$E = \frac{1}{2} m V_w^2 \quad (8)$$

$$m = 2\pi\rho R h V_w \quad (9)$$

Substituting (9) into (8), the expression for average power becomes (10).

$$P = \frac{E}{t} \quad (10)$$

But with the assumption of having constant wind velocity, time t can be neglected hence.

$$P = \frac{1}{2} (2\pi\rho R h V_w^3) \quad (11)$$

V_w is the exit wind velocity. In a wind turbine, the inlet and exit wind velocities are not the same. They are related by the equation $V_w = \frac{2}{3} V_i$, where V_i is the inlet wind velocity. Now:

$$P_{\max} = \frac{1}{2} [2\pi\rho R h (\frac{2}{3} V_i)^3] = \frac{1}{2} [(\frac{16}{27}) \rho R h V_i^3] \quad (12)$$

This power is known as the maximum power extractable from a wind turbine.

3.3. Power coefficient or Betz constant

To calculate the power coefficient, the ratio of the inlet and outlet wind velocity power has to be calculated.

$$\begin{aligned} P_{\max}/P_{\text{in}} &= \frac{16}{27} \left(\frac{[\frac{1}{2}(\frac{\rho A}{V_i^3})]}{[\frac{1}{2}(\frac{\rho A}{V_i^3})]} \right) \\ &= \frac{16}{27} \times 100 \\ &= 59\% \\ \text{where } P_{\text{in}} &= \frac{1}{2} (\rho A V_i^3) \text{ watt} \\ P_{\max} &= \frac{16}{27} [\frac{1}{2} (\rho A V_i^3)] \text{ watt} \end{aligned}$$

The above ratio of 59% is known as the maximum power coefficient and also known as the Betz constant. This constant gives the interpretation that it is a ratio of power extracted by the turbine over the total power that would exist at the same place before placing the wind turbine. The above torque is due to the circumferential force acting on the blade, and the torque is generated on the turbine.

3.4. Generator power output

The generator output is given by (13), and the P_{dc} depends on the generator efficiency and turbine efficiency, along with other design parameters given in Table 1.

$$P_{dc} = \frac{1}{2} (2\pi\rho R h V_i^3 \eta_G \eta_T) \quad (13)$$

Where P_{dc} = Generator power output, η_G = Generator efficiency, and η_T = Turbine efficiency. The generator power output is calculated for a wind speed ranging from 2.7 m/s to 12 m/s, with the following design parameters given in Table 1.

Table 1. Design parameters for power estimation

Parameters	Value	Parameters	Value
R	0.275 m	P	1.23 kg/m ³
H	1.03 m	η_G	0.9
V_i	2.7 m/s to 12 m/s	η_T	0.35

3.5. Maximum power output in a wind turbine

In this prototype, with V_i = (2.7 m/s to 12 m/s), R = 0.275 m, h = 1.03 m, and ρ = 1.23 kg/m³, the P_{\max} = 862.85 watt at 11 m/s, torque at 11 m/s is given by $T_{\max} = P_{\max} / \omega$ and $\omega = 2\pi R/60$ rad/s. Using the given expression, the estimated speed for 11 m/s = 382 rpm, ω = 40 rad/s and T_{\max} = 21.57 Nm. In Figure 14,

the power output of the generator is estimated for a range of wind speeds from 4 m/s to 12 m/s. The performance of the generator is demonstrated by the relationship between the wind speed and the maximum power of the wind turbine. A maximum power output of 862.85 watts at 11 m/s was achieved with the prototype model.

3.6. Generator output voltage

The output voltage for the design is shown in (14), where P = number of poles, ϕ = flux per pole, N = speed in rpm, and Z = number of conductors.

$$\text{Voltage } E = \frac{P\phi NZ}{60} \quad (14)$$

$$E = \frac{(2 \times 5 \times 10^{-3} \times 417 \times 800)}{60} = 55 \text{ V}$$

Both Figures 15 and 16 depict the voltage that was measured on the multimeter. Figure 16 also depicts the measured voltage in comparison with the theoretical value. The observed voltage is lower than the estimated value due to flux leakage, fluctuation in angular velocity, and drop in the conductor. The design parameters that were utilized for the purpose of theoretical estimation are presented in Table 2.

Table 2. Design parameters for voltage estimation

Parameters	Value	Parameters	Value
P	2	Φ	5 mWb
Z	800	N	94 to 417 rpm

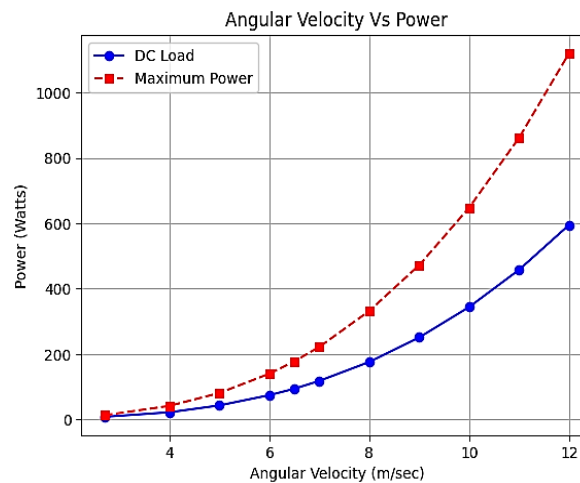


Figure 14. Power out of generator and maximum power out of turbine with angular velocity m/s



Figure 15. Measured voltage of VAWT

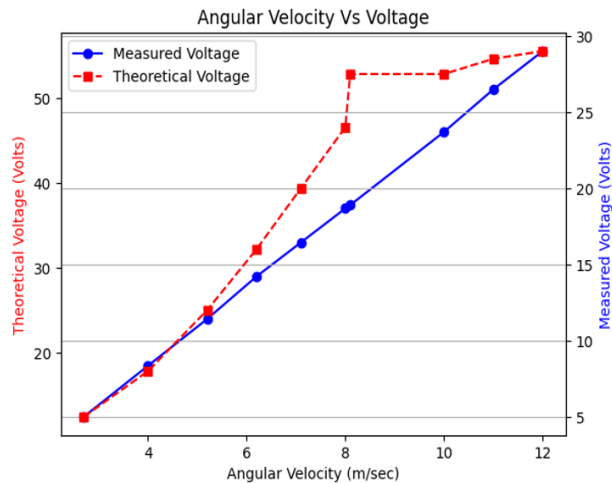


Figure 16. Voltage with angular velocity

4. CONCLUSION AND FUTURE SCOPE

This work has demonstrated the suitability of vehicle-mounted wind turbines for addressing power requirements in field and high-altitude applications, particularly in scenarios necessitating uninterrupted power supply, such as cut-off posts. Through the design and performance evaluation of the vertical axis wind turbine (VAWT) prototype, it was confirmed that the system meets the demanding operational needs of military vehicles. The compact, portable, and lightweight nature of the prototype facilitates easy mounting on vehicles, offering a practical solution for on-the-go power generation. Utilization of helical wind blades enables operation at lower wind speeds, while magnetic levitation reduces frictional losses, contributing to enhanced efficiency. The fiberglass material had reduced the weight of the blade, and with the optimization of the attack angle to get the maximum efficiency of 59% as per the Betz constant. Notably, for a wind speed range of 10 km/h to 40 km/h, the VAWT produces an output voltage ranging from 5 V to 55 V, with a maximum wind turbine power output of 1120 Watts at a wind speed of 12 m/s. The final generator output power obtained with the above wind turbine output of 1120 Watts is 352 Watts. The prototype achieved a maximum power output of 352 watts at 55 V, providing ample support for the DC load requirements of military vehicles stationed at cut-off posts. This underscores the efficacy of the vehicle-mounted wind turbine in fulfilling critical power needs in remote and challenging environments, showcasing its potential for practical deployment in real-world scenarios. Further optimization and refinement of the design hold promise for even greater efficiency and effectiveness in future iterations of the technology. Future work could focus on a transient analysis study that can be done to improve the reverse current protection circuit for better reliability and performance at cut-off post locations. The size can be reduced, making it suitable for different-sized vehicles with the same performance.

ACKNOWLEDGEMENT

We are thankful to the Military College of Electronics and Mechanical Engineering, Secunderabad, India, for providing test facilities.

FUNDING INFORMATION

This project was carried by the scholar without any financial support or scholarship from the university. The project idea was initiated based on the requirements of defense units located at the cut-off post, and a prototype model to demonstrate its performance and benefits for integrating into a defense vehicle to generate regenerative power. This was developed by the scholar without any funding. The testing of the prototype was carried out at the Military College of Electronics and Mechanical Engineering, Secunderabad, India.

AUTHOR CONTRIBUTIONS STATEMENT

This journal uses the Contributor Roles Taxonomy (CRediT) to recognize individual author contributions, reduce authorship disputes, and facilitate collaboration.

Name of Author	C	M	So	Va	Fo	I	R	D	O	E	Vi	Su	P	Fu
M. Priyadharsini	✓	✓	✓	✓	✓	✓	✓	✓	✓	✓				✓
Sunil Kumar Gupta		✓		✓		✓		✓	✓		✓	✓		
Manoj Gupta	✓		✓	✓		✓			✓		✓	✓	✓	

C : Conceptualization

M : Methodology

So : Software

Va : Validation

Fo : Formal analysis

I : Investigation

R : Resources

D : Data Curation

O : Writing - Original Draft

E : Writing - Review & Editing

Vi : Visualization

Su : Supervision

P : Project administration

Fu : Funding acquisition

CONFLICT OF INTEREST STATEMENT

Authors state no conflict of interest

DATA AVAILABILITY

The authors confirm that the data supporting the findings of this study are available within the article.




REFERENCES

- [1] S. Kahourzade, A. Mahmoudi, H. W. Ping, and M. N. Uddin, "A comprehensive review of axial-flux permanent-magnet machines," *Canadian Journal of Electrical and Computer Engineering*, vol. 37, no. 1, pp. 19–33, 2014, doi: 10.1109/CJECE.2014.2309322.
- [2] S. Yu *et al.*, "Researches on behavior of vibration in axial flux permanent magnet synchronous motor," in *Proceedings of the 11th International Conference on Electrical Machines and Systems, ICEMS 2008*, 2008, pp. 2789–2791.
- [3] D. Žarko, D. Ban, and T. A. Lipo, "Analytical calculation of magnetic field distribution in the slotted air gap of a surface permanent-magnet motor using complex relative air-gap permeance," *IEEE Transactions on Magnetics*, vol. 42, no. 7, pp. 1828–1837, 2006, doi: 10.1109/TMAG.2006.874594.
- [4] S. T. Boroujeni, A. A. Mohammadi, A. Oraee, and H. Oraee, "Approach for analytical modelling of axial-flux PM machines," *IET Electric Power Applications*, vol. 10, no. 6, pp. 441–450, 2016, doi: 10.1049/iet-epa.2015.0645.
- [5] B. Zhang, F. Wu, Z. Zhang, Z. Wei, and J. Xi, "3D magnetic field finite element analysis of dual-stator PM spherical motor," in *Proceedings of the 31st Chinese Control and Decision Conference, CCDC 2019*, 2019, pp. 5616–5620, doi: 10.1109/CCDC.2019.8832404.
- [6] W. Deng and S. Zuo, "Analytical modeling of the electromagnetic vibration and noise for an external-rotor axial-flux in-wheel motor," *IEEE Transactions on Industrial Electronics*, vol. 65, no. 3, pp. 1191–2000, 2018, doi: 10.1109/TIE.2017.2736487.
- [7] Z. Wu, Y. Fan, H. Wen, and D. Gao, "Vibration suppression of FSCW-IPM with auxiliary slots," in *2018 IEEE Energy Conversion Congress and Exposition, ECCE 2018*, pp. 3222–3227, 2018, doi: 10.1109/ECCE.2018.8557390.
- [8] C. Wang, X. Bao, S. Xu, Y. Zhou, W. Xu, and Y. Chen, "Analysis of Vibration and Noise for Different Skewed Slot-Type squirrel-cage induction motors," *IEEE Transactions on Magnetics*, vol. 53, no. 11, 2017, doi: 10.1109/TMAG.2017.2704038.
- [9] J. Li, H. X. Sun, and Y. Liu, "New rotor structure mitigating vibration and noise in switched reluctance motor," in *ICINA 2010 - 2010 International Conference on Information, Networking and Automation, Proceedings*, 2010, doi: 10.1109/ICINA.2010.5636789.
- [10] M. Sun, R. Tang, X. Han, and W. Tong, "Analysis and modeling for open circuit air gap magnetic field prediction in axial flux permanent magnet machines," in *Zhongguo Dianji Gongcheng Xuebao/Proceedings of the Chinese Society of Electrical Engineering*, 2018, pp. 1525–1533, doi: 10.13334/j.0258-8013.pcsee.170505.
- [11] P. Deshmukh, K. Gargelwar, K. Jadhav, P. Vankudre, and P. Sachin, "Vertical axis wind turbine using MAGLEV technology," *International Research Journal of Engineering and Technology (IRJET)*, vol. 4, no. 2, pp. 148–151, 2017, [Online]. Available: <https://irjet.net/archives/V4/i2/IRJET-V4I228.pdf>.
- [12] Q. Mo, J. Wen, X. Liu, and J. Wang, "The brake system and method of the small vertical axis wind turbine," in *Proceedings of the 2016 5th International Conference on Civil, Architectural and Hydraulic Engineering (ICCAHE 2016)*, Paris, France: Atlantis Press, 2016, doi: 10.2991/iccahe-16.2016.25.
- [13] S. V. Kozlov, E. A. Sirotkin, and E. V. Solomin, "Wind turbine rotor magnetic levitation," in *2016 2nd International Conference on Industrial Engineering, Applications and Manufacturing, ICIEAM 2016 - Proceedings*, 2016, doi: 10.1109/ICIEAM.2016.7911477.
- [14] U. Divakaran, A. Ramesh, A. Mohammad, and R. K. Velamati, "Effect of helix angle on the performance of helical vertical axis wind turbine," *Energies*, vol. 14, no. 2, 2021, doi: 10.3390/en14020393.
- [15] Q. Cheng, X. Liu, H. S. Ji, K. C. Kim, and B. Yang, "Aerodynamic analysis of a helical vertical axis wind turbine," *Energies*, vol. 10, no. 4, 2017, doi: 10.3390/en10040575.
- [16] K. Anupa, A. Faramarz, S. Yasushi, K. Ken, T. Shiro, and T. Junji, "Contactless magnetic braking control unit for small-scaled wind turbines for DC green house," in *34th International Technical Conference on Circuits/Systems, Computers and Communications, ITC-CSCC 2019*, 2019, doi: 10.1109/ITC-CSCC.2019.8793443.
- [17] N. Muhammad *et al.*, "Development of vertical axis wind turbine (VAWT) using magnetic levitation (MAGLEV)," *Journal of Advanced Research in Engineering Knowledge Journal homepage*, vol. 10, no. 1, pp. 23–35, 2020, [Online]. Available: www.akademiabaru.com/arek.html.
- [18] M. Nasiri, J. Milimonfared, and S. H. Fathi, "A review of low-voltage ride-through enhancement methods for permanent magnet synchronous generator based wind turbines," *Renewable and Sustainable Energy Reviews*, vol. 47, pp. 399–415, 2015, doi: 10.1016/j.rser.2015.03.079.
- [19] P. Ramesh and N. C. Lenin, "High power density electrical machines for electric vehicles-comprehensive review based on material technology," *IEEE Transactions on Magnetics*, vol. 55, no. 11, 2019, doi: 10.1109/TMAG.2019.2929145.
- [20] J. Y. Lee, J. H. Lee, and T. K. Nguyen, "Axial-flux permanent-magnet generator design for hybrid electric propulsion drone applications," *Energies*, vol. 14, no. 24, 2021, doi: 10.3390/en14248509.
- [21] G. Rodrigues Bruzina, A. J. S. Filho, and A. Pelizari, "Analysis and design of 3 kW axial flux permanent magnet synchronous motor for electric car," *IEEE Latin America Transactions*, vol. 20, no. 5, pp. 855–863, 2022, doi: 10.1109/TLA.2022.9693571.
- [22] X. Wang, T. Li, X. Cui, and X. Zhao, "Design and analysis of coreless axial flux permanent magnet machine with novel composite structure coils," *Energies*, vol. 15, no. 14, 2022, doi: 10.3390/en15145162.
- [23] L. Szabó and D. Fodor, "The key role of 3D Printing technologies in the further development of electrical machines," *Machines*, vol. 10, no. 5, 2022, doi: 10.3390/machines10050330.
- [24] X. Wei, M. L. Jin, H. Yang, X. X. Wang, Y. Z. Long, and Z. Chen, "Advances in 3D printing of magnetic materials: Fabrication, properties, and their applications," *Journal of Advanced Ceramics*, vol. 11, no. 5, pp. 665–701, 2022, doi: 10.1007/s40145-022-0567-5.
- [25] A. S. Holmes, G. Hong, and K. R. Pullen, "Axial-flux permanent magnet machines for micropower generation," *Journal of Microelectromechanical Systems*, vol. 14, no. 1, pp. 54–62, 2005, doi: 10.1109/JMEMS.2004.839016.
- [26] W. Geng and Z. Zhang, "Analysis and Implementation of new ironless stator axial-flux permanent magnet machine with concentrated nonoverlapping windings," *IEEE Transactions on Energy Conversion*, vol. 33, no. 3, pp. 1274–1284, 2018, doi: 10.1109/TEC.2018.2799172.
- [27] Y. Kaneko, T. Kitamura, K. Nakamura, and T. Takao, "Levitation force improvement by effective magnetic interaction in two magnetic levitation systems with HTS coil and bulks," *IEEE Transactions on Applied Superconductivity*, vol. 30, no. 5, pp. 1–6, Aug. 2020, doi: 10.1109/TASC.2020.2975171.
- [28] L. S. Mattos, E. Rodriguez, F. Costa, G. G. Sotelo, R. De Andrade, and R. M. Stephan, "MagLev-cobra operational tests," *IEEE Transactions on Applied Superconductivity*, vol. 26, no. 3, 2016, doi: 10.1109/TASC.2016.2524473.
- [29] Z. Deng, L. Wang, H. Li, J. Li, H. Wang, and J. Yu, "Dynamic studies of the HTS maglev transit system," *IEEE Transactions on Applied Superconductivity*, vol. 31, no. 5, 2021, doi: 10.1109/TASC.2021.3052452.
- [30] Z. Deng *et al.*, "A high-speed running test platform for high-temperature superconducting Maglev," *IEEE Transactions on Applied Superconductivity*, vol. 32, no. 4, pp. 1–5, Jun. 2022, doi: 10.1109/TASC.2022.3143474.




- [31] M. Igarashi *et al.*, “Persistent current HTS magnet cooled by cryocooler (1)-project overview,” *IEEE Transactions on Applied Superconductivity*, vol. 15, no. 2 Part II, pp. 1469–1472, 2005, doi: 10.1109/TASC.2005.849130.
- [32] Y. Fukasawa and H. Ohsaki, “Three-dimensional structure of magnetic field in the mixed- μ levitation system using bulk superconductors,” *IEEE Transactions on Applied Superconductivity*, vol. 9, no. 2 Part 1, pp. 980–983, 1999, doi: 10.1109/77.783462.
- [33] R. Shiraishi, K. Fujiyama, and H. Ohsaki, “Macroscopic magnetic flux motion in Y-Ba-Cu-O bulk superconductor during pulsed field magnetization,” *IEEE Transactions on Applied Superconductivity*, vol. 15, no. 2 Part III, pp. 3153–3156, 2005, doi: 10.1109/TASC.2005.848755.
- [34] K. Fujiyama, R. Shiraishi, and H. Ohsaki, “Influence of local superconducting properties on pulsed field magnetization of YBCO bulk superconductor,” *Physica C: Superconductivity and its Applications*, vol. 426–431, no. I, pp. 681–687, 2005, doi: 10.1016/j.physc.2005.01.044.
- [35] COMSOL, “AC/DC Module,” COMSOL Multiphysics, [Online]. Available: <https://www.comsol.com/acdc-module>.
- [36] Intertek, “JIS C 2504:2000 Soft Magnetic Irons,” Intertek Inform. [Online]. Available: http://www.intertekinform.com/en-gb/standards/jis-c-2504-2000-1199191_saig_jsa_jsa_2892272/.

BIOGRAPHIES OF AUTHORS






M. Priyadharsini    is currently a research scholar in the Department of Electrical Engineering at Poornima University, Jaipur, and an Associate Professor in the Department of Electrical Engineering at Military College of Electronics and Mechanical Engineering, Hyderabad, India, since 2002. She received her Bachelor's degree in Electrical and Electronics Engineering from the Government College of Technology in 1993, Tamil Nadu, and her master's in power electronics engineering from Pune University, Pune, in 1998. Her research interests include renewable energy systems for defense applications such as compressed air generator, vertical axis wind turbine, magnetic refrigeration, solar power, super capacitor with battery, piezoelectric power generation, and DC power distribution systems. She can be contacted at email: mpriyadharsini@gmail.com.



Dr. Sunil Kumar Gupta    received a B.Tech. in Electrical Engineering from Rajasthan University, Jaipur in 2003, an M.Tech. in power electronics, machine design, and drives in 2006 from MDU, and a Ph.D. in Electrical Engineering from MNIT, Jaipur in 2012. Currently, he is working as a Professor in the Electrical and Electronic Engineering Department at Poornima University, Rajasthan, India. He has over 20 years of academic, research, and administrative experience. Dr. Gupta has published more than 90 research papers in national and international journals and conferences, and he holds more than 35 patents. He has supervised 4 Ph.D. students and served as a mentor to 4 master's research candidates. He can be contacted at email: sunil.gupta@poornima.edu.in.



Dr. Manoj Gupta    did B.E. in Electrical Engineering, M.Tech., and Ph.D. from MNIT, Jaipur. He has 26 years of good experience in industry, research, and academia. Currently, he is working as Professor and Pro-President at Poornima University, Jaipur. He has made significant contributions to planning, designing, and implementing innovative teaching and learning processes, academic administration, and faculty training programs. He is an excellent motivator for both students and faculty. Under his supervision, 5 Ph.D. and 15 M.Tech. candidates have successfully completed their research work. Currently, he is supervising 4 Ph.D. scholars. Dr. Gupta has published over 45 research papers and has received various certificates and awards from both government and private organizations in recognition of his contributions. He can be contacted at email: manojg@poornima.edu.in.